

1 **The Lightning Differential Space Framework: Multiscale Analysis**
2 **of Stroke and Flash Behavior**

3
4
5
6

7 Yuval Ben Ami¹, Orit Altaratz¹, Yoav Yair², Ilan Koren¹

8 ¹Department of Earth and Planetary Sciences, The Weizmann Institute of Science, Rehovot, 7610001, Israel.

9 ²School of Sustainability, Reichman University, Herzliya, 4610101, Israel.

10
11 *Correspondence to:* [Ilan Koren \(ilan.koren@weizmann.ac.il\)](mailto:ilan.koren@weizmann.ac.il)

12
13 **Abstract.** Lightning flashes play a key role in the global electrical circuit, serving as markers of deep convection and
14 indicators of climate variability. However, this field of research remains challenging due to the wide range of physical
15 processes and spatiotemporal scales involved.

16 To address this challenge, this study utilizes the Lightning Differential Space (LDS), which maps lightning stroke
17 intervals onto a parameter space defined by their temporal and spatial derivatives.

18 Using data from the Earth Networks Total Lightning Network (ENTLN), we analyze the Number Distribution LDS
19 clustering patterns across specific seasons in three climatically distinct regions: a tropical rainforest region (the Amazon),
20 a subtropical marine environment (the Eastern Mediterranean Sea), and a mid-latitude continental region (the Great
21 Plains in the U.S.). The LDS reveals a robust clustering topography composed of “allowed” and “forbidden” -interval
22 ranges, which are consistent across regions, while shifts in cluster position and properties reflect the underlying regional
23 meteorological conditions.

24 As an extension of the LDS framework, we introduce the Current Ratio LDS, a new diagnostic for identifying flash
25 initiation by mapping the ratio of peak currents between successive strokes into the LDS coordinate space.
26 This space reveals a spatiotemporal structure that enables a clearer distinction between local and regional scales. It also
27 reveals a distinct cluster, suggesting a possible teleconnection between remote strokes, spanning tens to hundreds of
28 kilometers.

29 Together, the Number Distribution LDS and the novel Current Ratio LDS provide a scalable, data-driven framework for
30 analyzing and interpreting large datasets of CG lightning activity. This approach strengthens the ability to characterize
31 multiscale is suitable for comparing storm regions, validating lightning behavior, offers a framework for evaluating model
32 representations of stroke models, and flash processes, and provides a basis for developing diagnostics relevant to
33 operational monitoring and forecasting of lightning activity enhancing early warning systems.

34 **1. Introduction**

35 Cloud-to-Ground (CG) lightning flashes play a significant role in the global atmospheric ~~global~~ electric circuit (Siingh et
36 al., 2007), making it essential to understand their properties and driving mechanisms. In addition, studying CG flashes is
37 important for improving safety measures, as they pose severe hazards to life and infrastructure (Yair, 2018).

38 Thunderclouds are the building blocks of deep cloud systems. The size of a single Cumulonimbus typically ranges
39 ~~from~~between a few to a few tens of kilometers, depending on the season and location (Cotton et al. and Heever, 2011).
40 Their~~It's~~ lightning production rate varies between one flash every few seconds to one every few minutes, for a total
41 duration ranging from a few minutes up to \sim 1 h (Dwyer and Uman, 2014). The lightning production rate and ~~the~~ total
42 duration of ~~at~~the thundercloud's electrical activity depend on dynamic and microphysical processes, such as the
43 ~~updraft~~updraft's magnitude, the depth of the mixed-phase region, and the fluxes of liquid water, graupel, and ice mass
44 within the cloud (Deierling and Petersen, 2008; Deierling et al., 2008). A major part of ~~the~~ CG flashes (mainly negative
45 ones) consists of multi-stroke flashes, transferring charge to the ground through several return strokes, ~~some~~ of which
46 may follow different channels ~~and~~that contact the ground within a radius of \sim 10 km (Dwyer and Uman, 2014). The gaps
47 between ~~the~~ strokes are generally a few tens of milliseconds, and a CG flash has a total duration ~~of~~is 0.5–1 ~~seconds~~.
48 Studies have statistically shown that the first return stroke in a lightning flash generally has a stronger peak current than
49 ~~the~~ subsequent strokes (Chowdhuri et al., 2005; Poelman et al., 2013; Diendorfer et al., 2022). Positive CG flashes usually
50 consist of a single return stroke and have a higher peak current compared to negative ones (Rakov, 2003).

51 Many previous studies have examined the spatiotemporal properties of strokes and flashes and their relation to the micro
52 and macrophysical properties of thunderclouds (e.g., Mattos and Machado, 2011; Strauss et al., 2013). These properties
53 depend on geographic location, ~~the~~ season, and ~~the~~ type of convective system.

54 Observational studies also show that when thunderclouds cluster into an organized system, distinct spatial and temporal
55 lightning patterns can emerge. For example, in the case of Mesoscale Convective Systems (MCS), this can include a high
56 rate of cloud-to-ground (CG) flashes, a large horizontal extent of flashes, a bipolar pattern of ground contact points, and
57 other characteristics (MacGorman and Rust, 1998). On a larger scale, ~~several~~some studies suggest a coupling mechanism
58 between widely separated thunderclouds, leading to ~~a~~ synchronized lightning activity patterns (i.e., pattern
59 ~~teleconnection~~; Mazur, 1982; Vonnegut et al., 1985; Yair., et al 2006, 2009a; 2009).

60 Because lightning behavior depends~~Due to the dependence~~ on thunderstorm characteristics and environmental conditions,
61 robust characterization of investigating~~flash and~~ stroke and flash properties ~~require~~characteristics can greatly benefit
62 ~~from~~ large datasets that cover many storms.~~–~~ Lightning detection networks are valuable tools for this purpose, as they
63 provide~~utilizing~~ years of measurements collected over both land and ocean.

64 With advancements in measurement technology and retrieval algorithms, there is a growing interest in developing analysis
65 techniques that can extract new physical insights from existing long-term lightning network data. Traditional approaches
66 to processing lightning-network data typically begin by grouping individual strokes into flashes using predefined spatial–
67 temporal thresholds, a strategy employed in most operational flash algorithms. These approaches and their sensitivities
68 are reviewed in San Segundo et al. (2020). In contrast, the Lightning Differential Space (LDS) framework provides a
69 continuous, data-driven representation of stroke intervals without imposing a particular grouping scheme, allowing the
70 multiscale structure of electrical activity to emerge directly from the observed data.

71 Here, we extend the investigation of Ben Ami et al. (2022), who presented a unique differential space that reveals common
72 properties of time and distance intervals between successive strokes and used it, to characterize~~provide insights into~~ CG

73 flash activity on both thundercloud and cloud-system scales. Their work ~~was~~ focused on winter Cyprus-Lows in the
74 Eastern Mediterranean, analyzing ~50,000 CG strokes that were measured by the Israel Lightning Location System (ILLs,
75 Katz and Kalman, 2009), and introduced the LDS as a novel data-driven diagnostic framework to differentiate between
76 electrical events across a wide range of spatial and temporal scales.

77 In ~~this~~ the current study, we expand this investigation to three ~~regions of interest~~ Regions Of Interest (ROI), representing
78 different climatic regimes, using CG data collected by a global lightning detection network with a larger dataset per
79 region. ~~Beyond~~ In addition to extending the Number Distribution LDS to new environments, ~~we a main goal of this work~~
80 ~~is to~~ introduce the Current Ratio LDS (see section 2.3) – a new diagnostic framework for identifying flash initiation
81 intervals based on peak current sequencing.

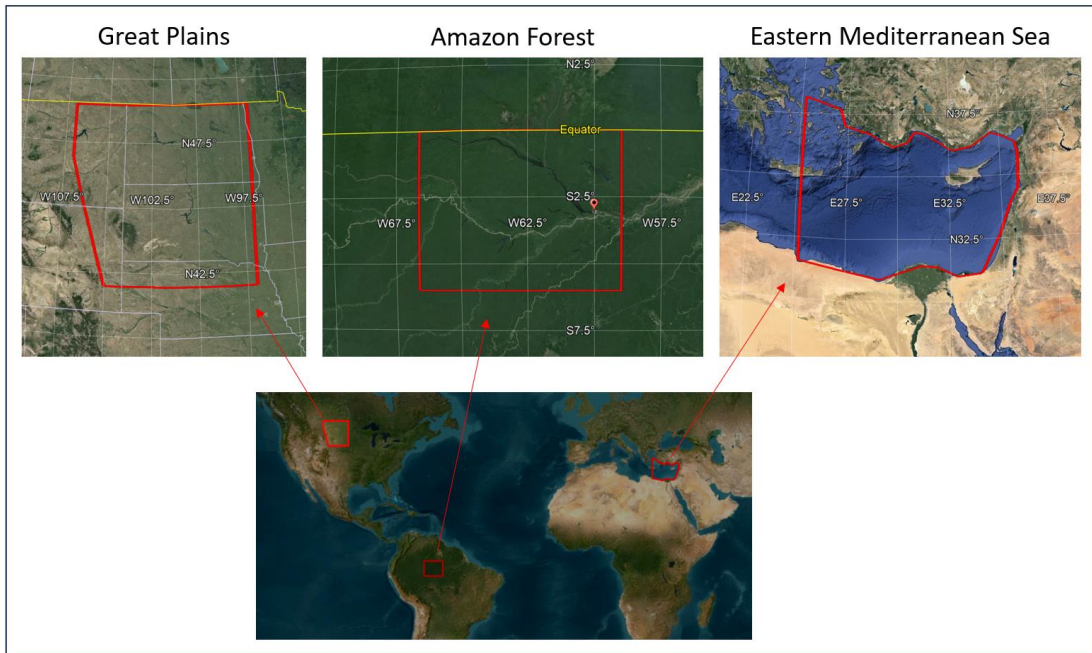
82

83

84 2. Data and Methods

85 2.1. Regions and Seasons

86 The three ROIs are (a) the Amazon (0°-6°S; 66.6°W-59°W), representing the tropics, (b) the Eastern Mediterranean Sea
87 (31°N-35°N; 25°E-35.5°E), representing the ~~subtropics, sub tropics~~ and (c) the northern part of the ~~U.S.~~ US Great Plains
88 (42°N-49°N; ~106°W-97°W), representing ~~the~~ mid-latitudes (Fig. 1). These ~~three~~ ROIs were selected ~~because for three~~
89 ~~main reasons:~~ (a) they represent three ~~distinct~~ different climate regimes. ~~Accordingly, we chose a few key parameters for~~
90 ~~general characterization of the atmospheric conditions: the Convective Available Potential Energy (CAPE), freezing-~~
91 ~~level height, and mixed-phase layer depth (estimated here as the difference between the cloud-top height and the freezing-~~
92 ~~level). These parameters have been shown in previous works to be highly correlated with the charge generation and flash~~
93 ~~rates in thunderstorms (Deierling and Petersen, 2008; Carey and Rutledge, 2000; Williams et al., 2002),~~ (b) they ~~exhibit~~
94 ~~intense seasonal lightning activity (experience intensive electrical activity during specific months (Cooper et al., 2019;~~
95 Oda et al., 2022; Altaratz et al., 2003; Jiang et al., 2006; Kaplan et al., 2022), and (c) ~~the ROI~~ ~~they~~ are ~~all~~ characterized
96 by ~~low-relief surface conditions that minimize local flat terrain which is important for minimizing the effect of~~ orographic
97 ~~triggering of convection, so that large-scale dynamics primarily influence the electrical activity on the analysis.~~ Using
98 ~~the~~ large ENTLN datasets, we analyze and compare the electrical activity in ~~these~~ ~~those~~ three regions.



100 Figure 1: Maps marking the study regions (© Google Maps 2015). The Amazon is bounded between 0°-6°S and 66.6°W-59°W, the
 101 Great Plains are bounded between 42°N-49°N, and ~106°W-97°W, and the Eastern Mediterranean Sea lies approximately between
 102 31°N-35°N and 25°E-35.5°E.

103 **2.1.1 The Amazon (Sep.–Nov.)**

104 During the wet season, lightning activity reaches its annual peak, as the Intertropical Convergence Zone migrates
 105 southward (Nobre et al., 2009), creating a belt of low pressure. At the same time, the upper levels are influencedcontrolled
 106 by the Bolivian High (Molion, 1993). Convection The convection is driven by local instability and moisture supplied by
 107 the forest (Wright et al., 2017). Additionally, low-level easterly winds transport humidity from the oceanOcean inland,
 108 furtherall supporting the development of intense convection and electrical activity. Other in the Amazon. Additional
 109 synoptic systems that support thunderstorm activity during the wet season include the South American Monsoon
 110 Systemsystem (Williams et al., 2002) and the South Atlantic Convergence Zone, which is a quasi-stationary band of deep
 111 clouds extendingthat extends from the Amazon Basin southeastward (Carvalho et al., 2004). During this season deep
 112 mixed-phase thunderclouds develop over the Amazon, with typical cloud-top height exceeding 15 km and a freezing level
 113 located around 5 km (Harris et al., 2000; Collow et al., 2016). CAPE typically has moderate values around 1000 J kg⁻¹
 114 during most of the season (Williams et al., 2002; Riemann-Campe et al., 2009) with maximum values of up to ~4000 J
 115 kg⁻¹ on rare occasions (Giangrande et al., 2017), conditions that support intense electrical activity (Williams et al., 2002;
 116 Andreae et al., 2004).

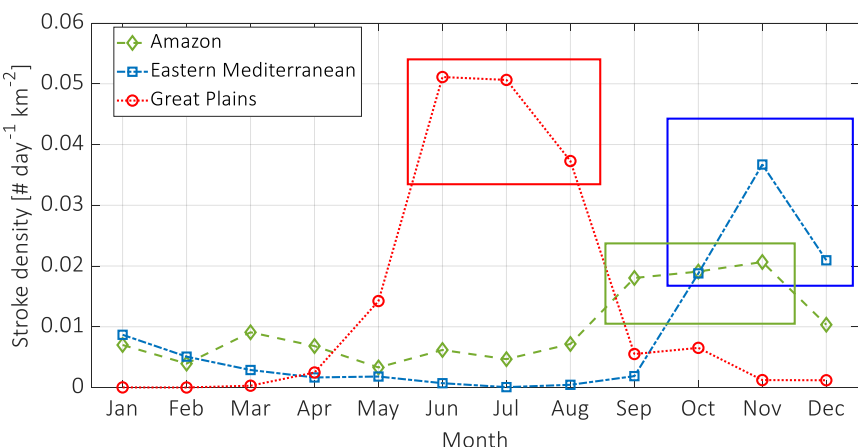
117 **2.1.2 The Eastern Mediterranean Sea (Oct.–Dec.)**

118 The most intense electrical activity in this region occurs during the boreal autumn and winter, driven mainly by mid-
 119 latitude cyclones. In these systems, continental cold air masses from Europe are advected toward the Mediterranean. As
 120 they propagate eastward, over the relatively warm sea, their moisture content increases, and the air massesthey become
 121 unstable. The low-pressure center is usually located near Cyprus, commonly referred to as a Cyprus Low (Shay-El and
 122 Alpert, 1991). Lows. Thunderclouds develop over the sea and near the coasteast, along cold fronts and post-frontal
 123 regions. A less frequent system is the Red Sea Trough (Ziv et al., -2005; Shalev et al., -2011), originating from the African
 124 monsoon over the Red Sea. When itis accompanied by an upper-level trough, it can support intense electrical activity
 125 over the Eastern Mediterranean Sea and neighboring countries, often leading to severe flooding. In contrast to the very
 126 deep convection in tropical or summertime mid-latitude environments, autumn and winter storms in this region have a

127 relatively shallow mixed-phase layer and exhibit low freezing-level heights. Cloud tops are between 7–11 km, with the
128 highest values typically occurring at the beginning of the season (Altaratz et al., 2001; Yair et al., 2009b), and the freezing
129 level is at ~2–3 km (Altaratz et al., 2001). The CAPE values are modest, typically between few hundreds and 1000 J kg⁻¹
130 characteristic of cold-season marine convection (Ben Ami et al., 2015).

131 2.1.3 The Northern Great Plains (Jun–Aug.)

132 During this time of year, this region is part of the corridor for passing MCSs, which are large clusters of
133 thunderstorms (Tuttle and Davis, 2006). MCSs often develop or intensify during the night, and typically form while they
134 develop along fronts (Ziegler and Rasmussen, 1998; Maddox et al., 1986) or drylines, which are the boundary between
135 moist air from the Gulf of Mexico and dry air from the desert Southwest (Scaff et al., 2021). MCSs can be sustained
136 by a low-level jet as well, which peaks after sunset and drives a southerly wind that supplies warm and humid air from
137 the Gulf of Mexico (Higgins et al., 1997). Summer convection in the Great Plains is typically associated with CAPE
138 values of ~1000–2500 J kg⁻¹ (Gizaw et al., 2021; Riemann-Campe et al., 2009), along with deep mixed-phase
139 thunderclouds with cloud-top height of ~18 km (Setvák et al., 2010). The freezing level is located at ~5 km (Wiens and
140 Suszczynsky, 2006) and there is usually strong vertical wind shear, reflecting the thermodynamic and dynamical structure
141 that favors the development of long-lived, highly electrified MCSs (Higgins et al., 1997; Tuttle and Davis, 2006). These
142 conditions contrast with the weak-shear, moist-tropical environment of the Amazon and define a distinct midlatitude
143 convective regime.



144

145 Figure 2: A histogram of the daily CG density (number of strokes per # day⁻¹ km⁻²) per month during 2020–2021. The selected months
146 for analysis are indicated, based on the highest/largest stroke density for each ROI.

147 2.2. Measurement System and Data

148 The CG stroke data used in this study were primarily retrieved by the ENTLN (Zhu et al., 2022), a global lightning
149 detection network. This network comprises more than 1,500 wideband (1 Hz–12 MHz) sensors, deployed
150 worldwide. Based on the detected electric-field waveform and the time-of-arrival technique, the network
151 estimates the pulse type (CG or intra-cloud; IC), ground-contact point, time of impact, peak current, and polarity.

152 Based on analyses of rocket-triggered and natural flashes, the reported CG stroke detection efficiency and
153 classification accuracy (estimated over the U.S.) are at least 96% and 86%, respectively. The median location error
154 is 215 m, and the absolute peak current error is 15%. A detailed description of the network performance can be found in
155 Zhu et al. (2022).

156 In this study, we use CG stroke data. ~~For each ROI, To minimize the impact of the interannual variability,~~ we focus on
 157 ~~thea~~ specific season ~~with for each ROI, selected based on~~ the highest stroke density ~~within 2020–2021 observed throughout~~
 158 ~~the years~~ (Fig. 2, Table 1), ~~ensuring that the LDS analysis is based on a large and representative sample of CG activity~~
 159 ~~for each region.~~ The total analyzed dataset includes 8,337,978 strokes, detected ~~over~~~~during~~ 182 days in the Amazon,
 160 118 days in the Eastern Mediterranean, and 175 days in the Great Plains, ~~during the selected seasons~~~~2020–2021~~.

161 To support and validate our ENTLN results, we use an additional CG dataset, measured by another lightning network,
 162 the Israeli Lightning Location System. At the time, the ILLS network included eight sensors, sensitive to the electric
 163 and/or magnetic ~~fields~~~~field~~ (Katz and Kalman, 2009). It detected 251,393 CGs ~~over~~~~during~~ 265 stormy days with diverse
 164 synoptic conditions, ~~during from Oct. to Dec. of, from 2004 to 2008, and 2010. Our ILLS dataset does not overlap~~
 165 with the ENTLN period (2020–2021), but it covers similar months ~~of~~~~along~~ the year and hence a similar type of synoptic
 166 systems, and can be used for validation. Due to the detection limits of the ILLS, the validation of the ENTLN analysis
 167 against the ILLS data was done in a different area ~~covering that covers~~ 250 km from the network center over the Eastern
 168 Mediterranean Sea and the adjacent land (Fig. S1). ~~This ILLS dataset~~~~data~~ was used in the previous work by Ben Ami et
 169 al. (2022).

170 *Table 1. Season, study area [km²], total number of analyzed days (with detected CG flashes), total number of analyzed hours, total*
 171 *number of detected CG strokes, number of strokes in clusters A, B+C, and D, and estimated flash density per ROI. (* Estimated from*
 172 *the ratio between the number of intervals B+C+1, to the area, and the number of days).*

173

	Amazon	Eastern Mediterranean	Great Plains	Total
Season	Sep.-Nov.	Oct.-Nov.	Jun.-Aug.	–
Area [km²]	563,270	566,010	562,730	1,692,010
# of days	182	118	175	475
Number of hours [#]	3,740	1,979	2,854	8,573
Number of CGs	1,974,302	1,790,482	4,573,194	8,337,978
Number of intervals in A [#]	674,538	863,374	869,395	2,407,307
Number of intervals in B+C [#]	1,282,533	894,543	3,642,374	5,819,450
Number of intervals in D [#]	17,230	32,564	61,424	111,221
Flash density [# km⁻² day⁻¹]*	0.013	0.013	0.037	–

174

175 2.3. Method

176 The CG stroke data ~~were~~~~was~~ sorted by the time of ground impact. Next, the time (dT) and distance (dR) intervals between
 177 consecutive strokes were calculated by subtracting the detection times and computing the distance between the
 178 geographical coordinates of each stroke pair. The number of events per interval range was projected onto a two-
 179 dimensional differential space, defined by dR and dT, termed the ~~Lightning~~~~Lighting~~ Differential Space (LDS), ~~hereafter;~~
 180 ~~this representation is~~ referred to as the Number Distribution LDS. ~~This~~ The density-based classification and visualization
 181 method, introduced by Ben Ami et al. (2022), requires no preprocessing of the data or the ~~use~~~~usage~~ of machine-~~learning~~
 182 algorithms, and offers an efficient way to extract statistically meaningful patterns from large lightning datasets. On one
 183 hand, it eliminates information ~~about~~~~on~~ the stroke ground-contact point and absolute time of incidence, and on the other,
 184 it clusters pairs of strokes with similar time and space interval properties.

185 To identify interval ranges with a higher likelihood of containing the initial stroke in a flash, we analyzed the peak currents
 186 of consecutive strokes by projecting the ratio of the absolute current value (polarity agnostic) between the 2nd and 1st

187 strokes in each pair onto the LDS coordinate system. This approach introduces the Current Ratio LDS. Because As we
188 anticipate that the peak currents tend toef strokes will decrease sequentially within a flash (Chowdhuri et al., 2005), the
189 Current Ratiocurrent ratio LDS is used to identify intervals that are more likely to contain the initial stroke in a flash.

190 **3. Results and Discussion**

191 We first examine the Number DistributionThe number distribution LDS, which provides a statistical view of how stroke

192 intervals populate the 2D dR–dT space. As shown in (Fig. 3a–c,) clusters stroke intervals with similar dR and dT cluster

193 into distinct "allowed" and "forbidden" interval ranges, revealing two dominant Two main clusters with a high probability

194 of occurrence, are indicated. Zero and low count values reveal the forbidden ranges of dR and dT intervals. This general

195 clustering topography is consistently observed across all three ROIs. However, shifts in cluster position and variations in

196 clustertheir characteristics reflect underlying meteorological differences among the three regions. This 2D representation

197 serves as the reference Number Distribution LDS, outlining the cluster structure that is examined in detail in the following

198 paragraphs.

199 The first cluster, marked as A, is characterized by short intervals between successive strokes both in time and space. For

200 all the ROIs, most of the events occur at in dT < 0.5 see, and they are it is limited to dR of a few kilometerskm and up to

201 a few tens of kilometerskm. The second cluster, marked as C, extends over longer dTs and larger dRs. Cluster A represents

202 time and space intervals between strokes in multiple-stroke flashes (multiplicity > 1), as it fits the characteristics of

203 consecutive CG strokes within a flash (Poelman, 2021; Wu et al., 2020). In contrast, cluster C groups the intervals between

204 the last stroke in one flash and the initial stroke in the next flash, initiated by a distant thundercloud, –in agreement with

205 Ben Ami et al. (2022). In the case of MCSsa MCSs’, which often spansspans over hundreds of kilometers, a subsequent

206 flashmayit could be initiated by a distant convective cell in the same wide-scale system. Note that the position of cluster

207 C is scale-dependent, and it is linked to the ROIsarea of each ROI. Nevertheless, we chose the areasarea of the ROIs to

208 be on the order of 500,000 km² (Table 1) to cover a synoptic scale so that the position of, henee cluster C location indicates

209 a typical scale of distances between electrical events at a synoptic (meso) scale.

210 In addition to the two dominant clusters, we also identify a ridge-like weak cluster, called here cluster B, representing

211 stroke intervals between consecutive flashes within a thundercloud. Unlike in Ben Ami et al. (2022), who analyzed the
212 smaller ILLS dataset, cluster B does not exhibithas no clear centers across all ROIs. This is due to the larger dataset

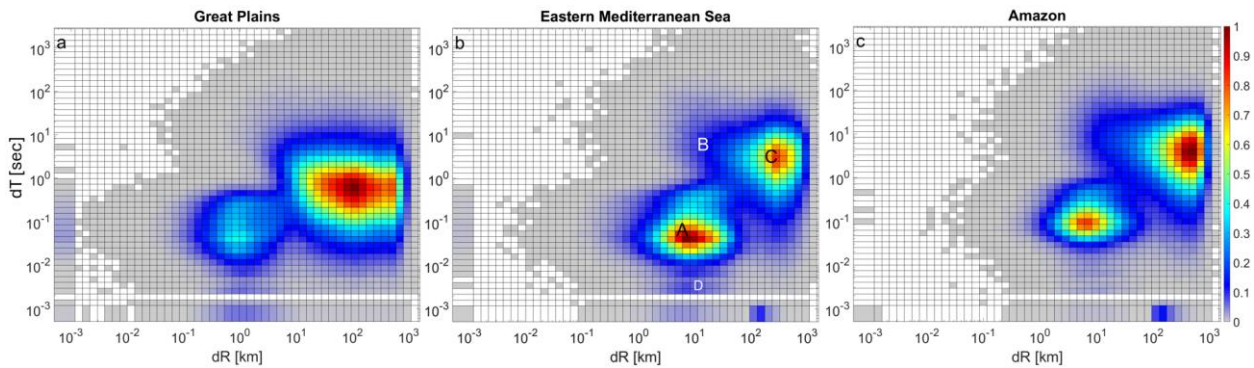
213 available fromof the ENTLN analyzed here and the inclusion of various synoptic conditions. The presence of B in the

214 ENTLN data is illustrated in the Supplementary Materialssupplementary section (Fig. S2) for a smaller dataset. To further

215 validate our findings, we analyzed the ILLS data for the Eastern Mediterranean (Fig. S1). The results indicate a similar

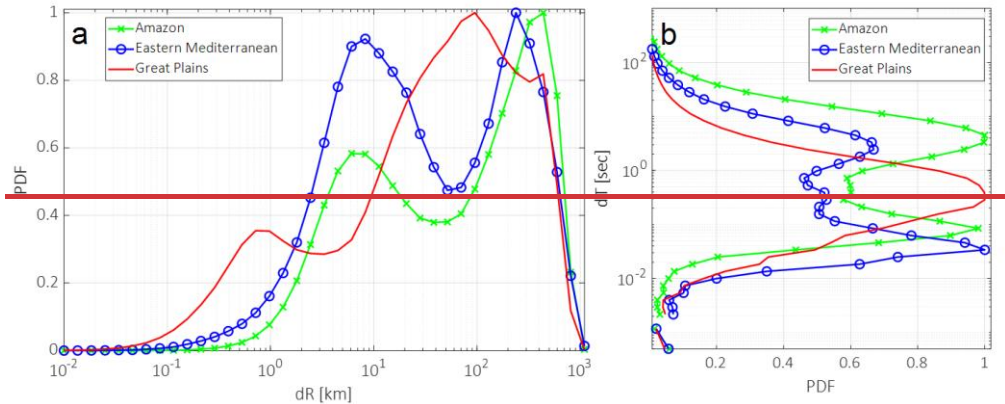
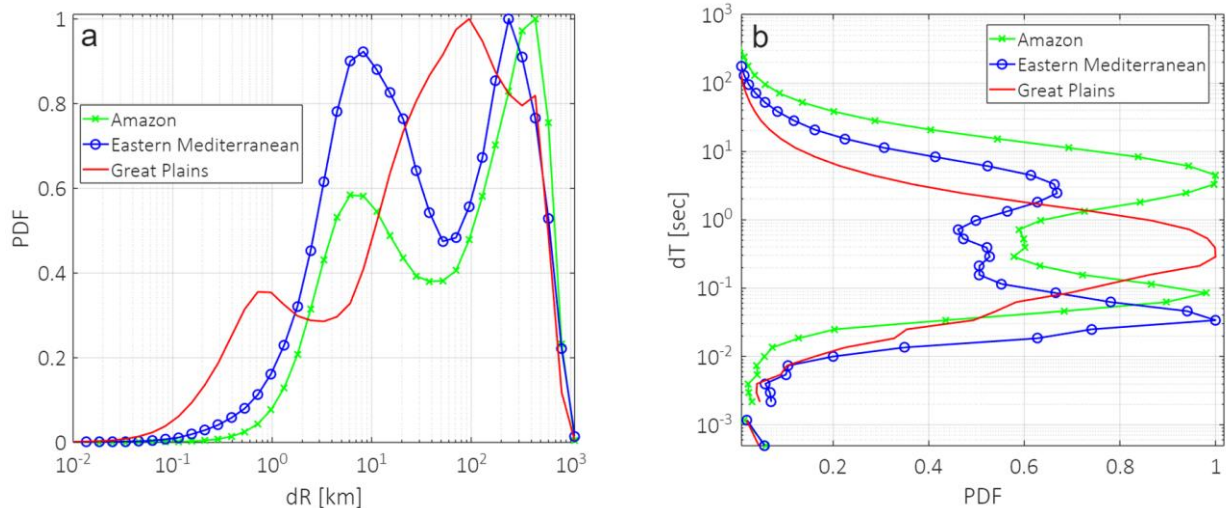
216 manifestation of B, appearing as a ridge in the Number Distributionnumber distribution LDS, without a distinct center

217 (see Fig. S3).



220 Figure 3: Number [Distribution](#)~~distribution~~ LDS~~PDF~~ PDF of the dR and dT intervals between consecutive strokes, normalized by the
 221 maximum [number of counts](#), for (a) the Great Plains, (b) [the](#) Eastern Mediterranean, and (c) the Amazon. The locations of clusters A~~–~~
 222 –D are illustrated in panel (b). Intervals with PDF < 0.025 are marked in gray.

224 Figure 4 shows the projection of the PDFs (from Fig. 3) onto the dR (X) and dT (Y) axes. The projection on the dT axis
 225 (Fig. 4b) clarifies that in the Great Plains, there is no temporal separation between clusters A and C, [i.e., that is,](#) between
 226 events occurring at the cloud scale and at the cloud~~–~~system scale. This contrasts with the well-defined temporal separation
 227 between clusters A and C observed in the other two regions, the Eastern Mediterranean and the Amazon. [This lack of](#)
 228 [separation, together with](#)~~This, and~~ the relatively shorter dTs of cluster C (between ~0.1~~–~~2.4s), [is consistent with the](#)
 229 [higher CAPE values and deeper clouds in the Great Plains, which support stronger updrafts and enhanced charge](#)
 230 [separation, leading to shorter stroke-to-stroke intervals. It is also reflected in](#)~~4~~[see](#)~~4~~ [are a result of](#) the high flash density
 231 in [this](#)~~the Great Plains~~ region ($0.037 \text{ km}^{-2} \text{ day}^{-1}$, [see](#) Table 1). [This density is](#) about three times greater than the flash
 232 density in the Eastern Mediterranean and the Amazon ($0.013 \text{ km}^{-2} \text{ day}^{-1}$, Table 1). This finding is supported by Kastman
 233 et al. (2017), who report a high CG flash rate for a certain type of MCSs passing over the Great Plains during this season.
 234 The elevated flash density in this region is likely related to the frequent occurrence of MCSs and [other](#) long-lived
 235 mesoscale systems, which are characterized by [a](#) high frequency of electrical events and hence shorter intervals between
 236 flashes, [thereby shifting cluster C toward shorter dTs.](#)

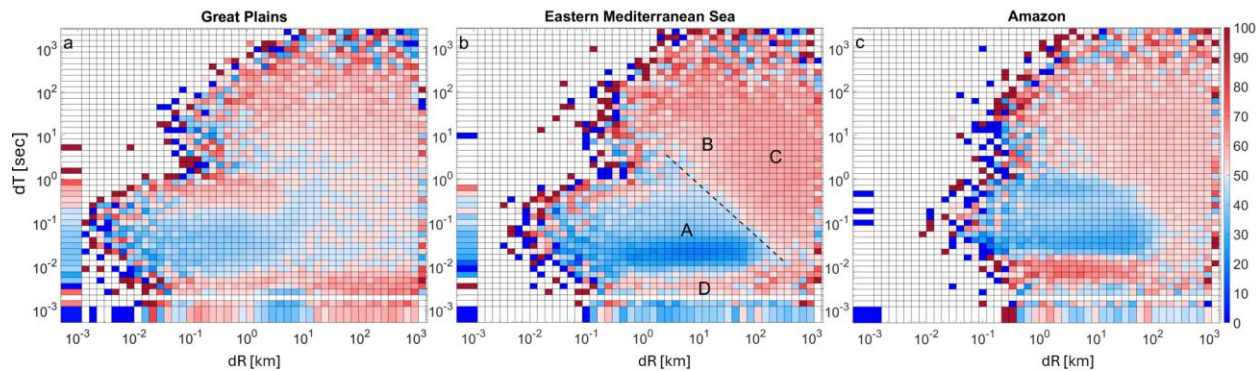
240 Figure 4: Projections of the [Number Distribution](#) LDS in Fig. 3 onto the dR (a) and dT (b) axes.

242 Additional differences between the ROIs can be recognized when examining the clusters' [positions](#) along the dR
 243 axis. While in the Amazon and the Eastern Mediterranean, cluster C is centered around 250–400 km, in the Great Plains
 244 it is located at a shorter distance of ~100 km (Fig. 3 and Fig. 4a). This indicates a smaller characteristic distance, at the
 245 cloud-system scale, between electrical events in the Great Plains. In addition, the characteristic dR of cluster A is different:
 246 it is located around 7 km in the Eastern Mediterranean and the Amazon and around ~1 km in the Great Plains, suggesting
 247 a smaller, [denser](#) [ground-impact](#) radius of strokes within a flash. Poelman et al. (2021) observed a similar tendency for
 248 shorter distances between [ground-strike](#) points within a flash over the [U.S.](#) [US](#) (Florida) when [compared with](#) [examined](#)
 249 [against](#) a few other regions in Europe, Brazil, and South Africa. Their reported median value of 1.3 km is comparable to
 250 our findings for the Great Plains. Nevertheless, we cannot rule out that this is a manifestation of smaller location errors
 251 over the Great Plains due to the higher density of ENTLN sensors in the [U.S.](#) [US](#). The denser sensor coverage in this region
 252 results in better detection accuracy and improved spatial resolution, which could contribute to the shorter dR values
 253 observed in [cluster](#) [Cluster](#) A (Fig. 3–4).

254 [Using the Current Ratio LDS](#) introduced in Sect. 2.3, [Another analysis](#) we [analyze](#) [performed](#) [to](#) [study](#) [stroke](#) [characteristics](#)
 255 [in](#) [the](#) [different](#) [ROIs](#) [is](#) the projection of consecutive strokes' peak current ratio [onto](#) [the](#) [LDS](#) [coordinate](#) [system](#) (Fig.
 256 5). [That](#) [is](#), [the](#) [ratio](#) [between](#) [the](#) [absolute](#) [current](#) [of](#) [the](#) [2nd](#) [and](#) [the](#) [1st](#) [stroke](#) [in](#) [each](#) [of](#) [the](#) [pairs](#). Given that statistically
 257 the peak current of CG strokes decreases monotonically with their order within a flash, we [identify](#) [identified](#) interval

ranges that are more likely to represent the initial stroke in a flash (see schematic illustration in Fig. S4). Complementary to the Number Distributionnumber distribution LDS in Fig. 3, we find that the Current Ratiocurrent ratio LDS functions as like a partitioning algorithm rather than a clustering method. It separates the space into dR and dT interval ranges, in whichwhere the current amplitude of the succeeding stroke is statistically larger (reddish) or smaller (bluish) than that of the preceding one. In agreement with the interpretation of the clusters inon the number-distribution LDS, the 2nd stroke in a pair in clusters B and C, the 2nd stroke in a pair is more likely to have a stronger peak current (reddish) and is therefore, hence assumed to be the initial stroke in a new, different flash. Accordingly, in cluster A, representing consecutive strokes in multiple-stroke CG flashes, the 2nd stroke in a pair is more likely to have a smaller peak current (bluish).

267



268 **Figure 5: Current Ratio LDS (based on the ratio between the absolute peak current of 2nd and 1st strokes in each pair) for (a) the Great**
 269 **Plains, (b) the Eastern Mediterranean, and (c) the Amazon. Reddish intervals indicate a stronger amplitude of the 2nd stroke in more**
 270 **than 50% of the pairs, while the bluish intervals show the opposite. The location of clusters A–D is illustrated on panel b. The boundary**
 271 **between the main reddish and bluish regions is illustrated by the dashed line in panel b.**

273

274 This clear and sharp separation into distinct red and blue regions on the Current Ratiocurrent ratio LDS is consistent and
 275 repeatable across the three ROIs, although it is less distinct in the Great Plains. A similar separation between initial and
 276 successive strokes within a flash, again formingclearly separated into red and blue zones, can be seen in the Current
 277 Ratiocurrent ratio LDS produced from the ILLS network data (Fig. S5), which iswas used as a validation dataset. The
 278 agreement between the two independent detection systems supports the robustness of our findings and indicates, that this
 279 is a consistent property of lightning discharge sequences in thunderstorms.

280 The diagonal boundaryborderline between events is illustrated in Fig. 5b. It is not a strict physical boundary but a
 281 statistical partition that reflects the dominant stroke-pair dynamics: initial strokes (reddish) vs. inter-flash (subsequent)
 282 strokes (bluish). It indicates that the shorter the distance between strokes, the longer the delay to the next flash. Focusing
 283 on time scales of a few seconds and distances of a few tens of kilometerskm, Zoghzogh et al. (2013) reported a similar
 284 inverse relation between the distance and the time to the next stroke. Here, we demonstrate that this relationship may also
 285 apply on a sub-second time scaletimescale and across tens of kilometers.

286

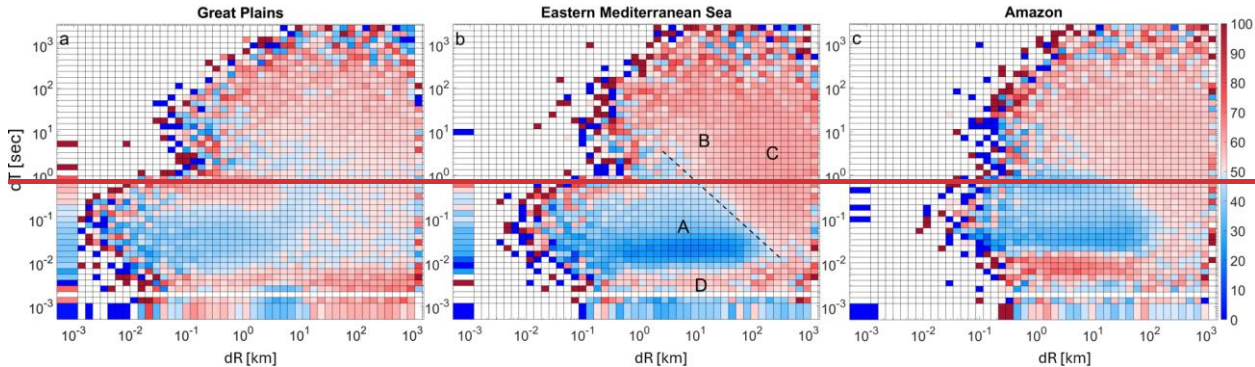


Figure 5: Current ratio (between the absolute current of 2nd and 1st strokes in each pair) LDS for (a) the Great Plains, (b) Eastern Mediterranean, and (c) the Amazon: The percent of pairs with stronger successive stroke peak current (2nd in pair). Reddish intervals indicate a stronger amplitude of the 2nd stroke in more than 50% of the pairs, while the bluish intervals show the opposite. Analogous to how Fig. 4 summarizes the Number Distribution LDS in Fig. 3, Fig. 6 provides one-dimensional summaries that clarify the patterns seen in the two-dimensional current-ratio LDS in Fig. 5. Because the current-ratio is not additive, these summaries are computed as the median value along each axis rather than as projections. They highlight how the likelihood of a stronger/weaker subsequent stroke varies systematically with distance (Fig. 6a) and time interval (Fig. 6b) and demonstrate the contrasting behavior of cluster A versus clusters B and C more clearly. The location of clusters A–D is illustrated on panel b. The borderline between the main reddish and bluish regions is illustrated by the dashed line on panel b.

A unique and new feature, that appears in the Current Ratio LDS of the three ROIs, is cluster D (marked in Fig. 5b and 6b). This cluster is characterized by very short dTs (on the order of <0.02 s), which are shorter than the characteristic dT of cluster A, and a very wide range of dRs, ranging from hundreds of meters to hundreds of kilometers. Containing less than 2% of the data, cluster D is not distinct when examining the number of events on the Number Distribution LDS (Fig. 3). Its topography becomes visible only when examining the Current Ratio LDS (Fig. 5).

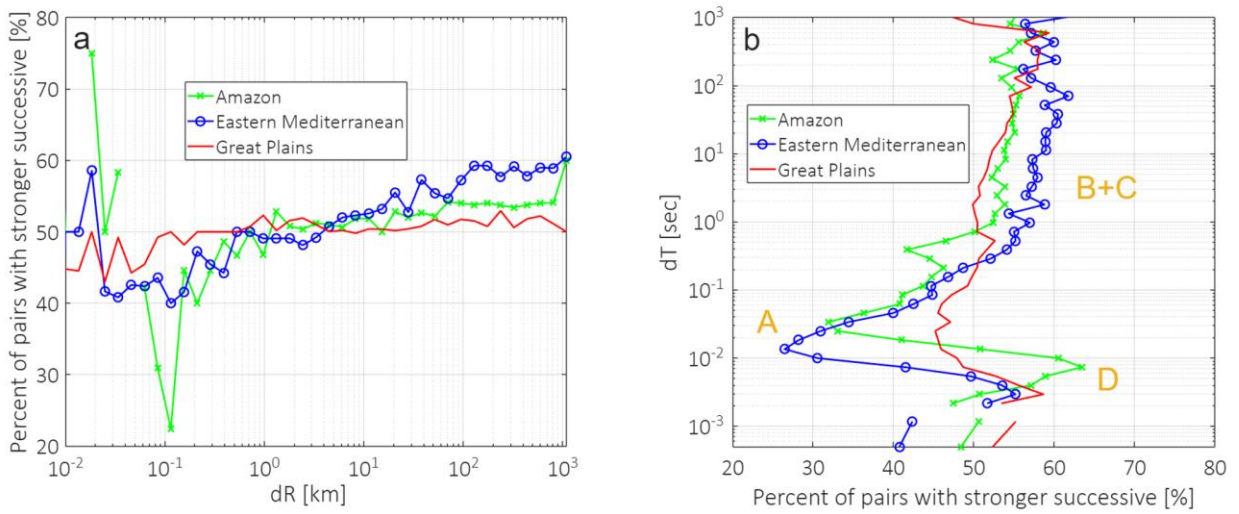


Figure 6: Median Current Ratio LDS projected onto the dR (a) and dT (b) axes, respectively, corresponding to the two-dimensional distributions shown in Fig. 5a–c. The position of cluster A–D is indicated in panel b.

308 The validation analysis, similar to the main analysis but using the ILLS network data, reveals a similar D-cluster D (Fig. 309 S5). This supports the robustness of this finding and eliminates the possibility that cluster D is an artifact of the ENTLN 310 retrieval algorithm.

311 The high percentage of a stronger peak current of the 2nd stroke in a pair in cluster D (similar to clusters B and C, also 312 marked in Fig. 6b) indicates that these stroke pairs they are probably the initial strokes in flashes. However, cluster D 313 spans a wide range of distances (dRs). For short distances, up to ten or a few tens of kilometers km, it may indicate 314 electrical events within the same thundercloud. It appears when a consecutive stroke in a multiple-stroke flash is more 315 intense than the previous one, as expected for ~30% of the flashes (Diendorfer et al., 2022). In this regard that respect, it 316 is notable that interesting to see the clustering of such events occurs at shorter dTs than the typical inter-stroke dT intervals 317 in cluster A. The part of cluster D that pertains to much longer dRs indicates electrical events involving of two strokes that 318 take place nearly simultaneously but at locations that are tens to and hundreds of kilometers apart km away. Several studies 319 have suggested a similar temporal sequence of remote flashes. Although the exact mechanism is yet to be elucidated, 320 several processes have been proposed, suggesting that their nearly simultaneous occurrence is not a pure coincidence and 321 that there is a physical mechanism that ties these remote strokes together. Füllekrug (1995), Ondrášková et al. (2008), and 322 Yair et al. (2006) have suggested triggering by the Schumann resonance. Later, Yair et al. (2009a, 2009) proposed a 323 theoretical model in by which a lightning flash may enhance the electric field in neighboring cells, as a function of the 324 distance between them, potentially triggering a near-simultaneous simultaneously flash in a remote (mature) thundercloud. 325 Here, using only data from a lightning location network, we cannot confirm or not rule out the those lightning-triggering 326 mechanisms that may explain the part of cluster D with longer dRs.

327

328 4. Summary

329 This study focuses on the parameters of CG flashes within individual thunderclouds and cloud systems. We analyzed the 330 distribution number of stroke intervals as expressed within the Lightning and the peak current ratio between successive 331 strokes in the Lightning Differential Space (LDS), using both the Number Distribution LDS domain (Ben Ami et al., 332 2022) and the newly introduced Current Ratio LDS.). Three distinct climatic regions were examined: the tropics 333 (Amazon), the subtropics (Eastern Mediterranean Sea), and the mid-latitudes (Great Plains in the U.S.), USA.

334 By clustering similar events, the Number Distribution LDS enables differentiation between electrical events on the scale 335 of a single thundercloud versus those of a larger cloud system. The identified clusters represent initial strokes in individual 336 thunderclouds (ridge B), initial strokes in a cloud system -(cluster C), and successive strokes in multi-stroke flashes 337 (cluster A).

338 The Current Ratio LDS provides an additional emerges as a new key diagnostic tool. It sharply and consistently 339 discriminates between interval ranges that are more likely to contain initial strokes in flashes and those that are not. A 340 fourth cluster (cluster D) indicates occurrences of successive strokes striking the ground up to tens to hundreds of 341 kilometers apart, yet within just a few milliseconds of each other, suggesting possible long-range interaction between 342 thunderstorms. In the present study, we focus on CG lightning strokes because the characteristic times of IC lightning 343 differ, and hence the application of the LDS framework to this type of data requires further investigation in future work.

344 Overall, the LDS provides a scalable and objective framework for analyzing large lightning big datasets of stroke row 345 data and interpreting their multiscale nature lightning activity. It reveals coherent spatiotemporal patterns and regional 346 similarities in flash behavior. These capabilities support scientific and This method applies to a range of operational

347 applications, such as comparison with cloud-resolving model outputs and including comparative analysis of storm regions,
348 lightning-parameterization schemes model validation, and the provision of a diagnostic approach that may support
349 probabilistic flash nowcasting or enhancement of early-warning tools systems.

350

351

352

353 **Code availability**

354 The code used in this study is not publicly available, as it depends on proprietary lightning stroke data that are not
355 openly accessible. As such, the code cannot be executed or validated independently without access to the licensed
356 datasets.

357 **Data availability**

358 The lightning stroke data used in this study were obtained from commercial sources under license and are not publicly
359 available. Access to these data is restricted by data use agreements with the Earth Networks Total Lightning Network
360 (ENTLN) and the Israel Lightning Location System (ILLS).

361 **Interactive computing environment**

362 No interactive computing environment is available for this study.

363 **Sample availability**

364 No physical samples were used or generated in this study.

365 **Author contribution**

366 IK and YBA develop the concept and OA prepared the manuscript with contributions from all co-authors. YY provided
367 the datasets, and the method. YBA performed the analysis. YY provided the datasets. YBA, OA, YY and IK, wrote the
368 manuscript.

369 **Competing interests**

370 The contact author has declared that none of the authors has any competing interests.

371 **Disclaimer**

372 The views and conclusions expressed in this article are solely those of the authors and do not necessarily reflect the views
373 of the data providers. The authors have no financial or commercial interest in the data sources used in this study.

374 **Acknowledgement**

375 N\A

376 **Financial support**

377 This project has received funding from the European Research Council (ERC) under the European Union's Horizon 2020
378 research and innovation programme (grant agreement No 810370), and YY was supported by the Israeli Science
379 Foundation grant ISF 1848/20.

380 **Review statement**

381 This paper is currently under review for the journal Atmospheric Measurement Techniques.

382 **References**

- 383 1. [Altaratz, O., Levin, Z. and Yair, Y.: Winter thunderstorms in Israel: A study with lightning location systems and weather radar. Monthly weather review, 129\(5\), pp.1259-1266, https://doi.org/10.1175/1520-0493\(2001\)129%3C1259:WTIIAS%3E2.0.CO;2, 2001.](https://doi.org/10.1175/1520-0493(2001)129%3C1259:WTIIAS%3E2.0.CO;2)
- 386 2. [Altaratz, O., Levin, Z., Yair, Y., and Ziv, B.: Lightning activity over land and sea on the eastern coast of the Mediterranean, Monthly Weather Review 131, no. 9, 2060-2070, https://doi.org/10.1175/1520-0493\(2003\)131<2060:LAOLAS>2.0.CO;2, 2003.](https://doi.org/10.1175/1520-0493(2003)131<2060:LAOLAS>2.0.CO;2)
- 389 3. [Andreae, M.O., Rosenfeld, D., Artaxo, P., Costa, A.A., Frank, G.P., Longo, K.M. and Silva-Dias, M.A.F.D.: Smoking rain clouds over the Amazon. science, 303\(5662\), pp.1337-1342, https://doi.org/10.1126/science.1092779, 2004.](https://doi.org/10.1126/science.1092779)
- 392 4. [Ben Ami, Y., Altaratz, O., Yair, Y. and Koren, I.: Lightning characteristics over the eastern coast of the Mediterranean during different synoptic systems. Natural Hazards and Earth System Sciences, 15\(11\), pp.2449-2459, https://doi.org/10.5194/nhess-15-2449-2015, 2015.](https://doi.org/10.5194/nhess-15-2449-2015)
- 395 5. [Ben Ami, Y., Altaratz, O., Koren, I., and Yair, Y.: Allowed and forbidden zones in a Lightning-strokes spatio-temporal differential space, Environmental Research Communications, 4\(3\), p.031003, DOI 10.1088/2515-7620/ac5ec2, 2022.](https://doi.org/10.1088/2515-7620/ac5ec2)
- 398 6. [Carey, L.D. and Rutledge, S.A.: The relationship between precipitation and lightning in tropical island convection: A C-band polarimetric radar study. Monthly weather review, 128\(8\), pp.2687-2710, https://doi.org/10.1175/1520-0493\(2000\)128%3C2687:TRBPAL%3E2.0.CO;2, 2000.](https://doi.org/10.1175/1520-0493(2000)128%3C2687:TRBPAL%3E2.0.CO;2)
- 401 7. [Carvalho, L.M., Jones, C. and Liebmann, B: The South Atlantic convergence zone: Intensity, form, persistence, and relationships with intraseasonal to interannual activity and extreme rainfall, Journal of Climate, 17\(1\), pp.88-108., https://doi.org/10.1175/1520-0442\(2004\)017%3C0088:TSACZI%3E2.0.CO;2, 2004.](https://doi.org/10.1175/1520-0442(2004)017%3C0088:TSACZI%3E2.0.CO;2)
- 404 8. [Chowdhuri, P., Anderson, J.G., Chisholm, W.A., Field, T.E., Ishii, M., Martinez, J.A., Marz, M.B., McDaniel, J., McDermott, T.E., Mousa, A.M., and Narita, T.: Parameters of lightning strokes: A review. IEEE Transactions on Power Delivery, 20\(1\), pp.346-358, doi:-10.1109/TPWRD.2004.835039, 2005.](https://doi.org/10.1109/TPWRD.2004.835039)
- 407 9. [Collow, A.B.M., Miller, M.A. and Trabachino, L.C.: Cloudiness over the Amazon rainforest: Meteorology and thermodynamics. Journal of Geophysical Research: Atmospheres, 121\(13\), pp.7990-8005, https://doi.org/10.1002/2016JD024848, 2016.](https://doi.org/10.1002/2016JD024848)

410 5. Cooper, M.A., and Holle, R.L.: Global lightning distribution. Reducing Lightning Injuries Worldwide, pp.107-
411 114, <https://doi.org/10.1109/TPWRD.2004.835039>, 2019.

412 6.10. Cotton, W.R., Bryan, G., and van den Heever, S.C.: Cumulonimbus clouds and severe convective
413 storms, In International geophysics (Vol. 99, pp. 315-454), Academic Press, <https://doi.org/10.1016/S0074->
414 6142(10)09914-6, 2011.

415 7.11. Deierling, W., and Petersen, W.A.: Total lightning activity as an indicator of updraft characteristics,
416 Journal of Geophysical Research: Atmospheres, 113(D16), <https://doi.org/10.1029/2007JD009598>, 2008.

417 8.12. Deierling, W., Petersen, W.A., Latham, J., Ellis, S., and Christian, H.J.: The relationship between
418 lightning activity and ice fluxes in thunderstorms, Journal of Geophysical Research, Atmospheres, 113(D15),
419 <https://doi.org/10.1029/2007JD009700>, 2008.

420 13. Dwyer, J.R., and Uman, M.A.: The physics of lightning, Physics Reports, 534(4), pp.147-241,
421 <http://dx.doi.org/10.1016/j.physrep.2013.09.004>, 2014.

422 9.14. Diendorfer, G., Bologna, F.F., and Engelbrecht, C.S.: A review of the relationship between peak
423 currents of the first and subsequent strokes in the same flash, In 2022 36th International Conference on Lightning
424 Protection (ICLP) (pp. 10-13), IEEE, <https://doi.org/10.1109/ICLP56858.2022.9942502>, 2022.

425 10. Dwyer, J.R., and Uman, M.A.: The physics of lightning, Physics Reports, 534(4), pp.147-241, 2014.

426 11.15. Füllekrug, M.: Schumann resonances in magnetic field components, Journal of Atmospheric and
427 Terrestrial Physics, 57(5), pp.479-484, [https://doi.org/10.1016/0021-9169\(94\)00075-Y](https://doi.org/10.1016/0021-9169(94)00075-Y), 1995.

428 16. Giangrande, S.E., Feng, Z., Jensen, M.P., Comstock, J.M., Johnson, K.L., Toto, T., Wang, M., Burleyson, C.,
429 Bharadwaj, N., Mei, F. and Machado, L.A.: Cloud characteristics, thermodynamic controls and radiative impacts
430 during the Observations and Modeling of the Green Ocean Amazon (GoAmazon2014/5)
431 experiment. Atmospheric Chemistry and Physics, 17(23), pp.14519-14541, <https://doi.org/10.5194/acp-17->
432 14519-2017, 2017.

433 17. Gizaw, M.S., Gan, T.Y., Yang, Y. and Gan, K.E. Changes to the 1979–2013 summer convective available
434 potential energy (CAPE) and extreme precipitation over North America. Physics and Chemistry of the Earth,
435 Parts A/B/C, 123, p.103047, <https://doi.org/10.1016/j.pce.2021.103047>, 2021.

436 18. Harris Jr, G.N., Bowman, K.P. and Shin, D.B.: Comparison of freezing-level altitudes from the NCEP reanalysis
437 with TRMM precipitation radar brightband data. Journal of climate, 13(23), pp.4137-4148, 2000.

438 19. Higgins, R.W., Yao, Y., Yarosh, E.S., Janowiak, J.E., and Mo, K.C.: Influence of the Great Plains low-
439 level jet on summertime precipitation and moisture transport over the central United States, Journal of Climate,
440 10(3), pp.481-507, [https://doi.org/10.1175/1520-0442\(1997\)010%3C0481:IOTGPL%3E2.0.CO;2](https://doi.org/10.1175/1520-0442(1997)010%3C0481:IOTGPL%3E2.0.CO;2), 1997.

441 20. Jiang, X., Lau, N.C. and Klein, S.A.: Role of eastward propagating convection systems in the diurnal cycle and
442 seasonal mean of summertime rainfall over the US Great Plains. Geophysical Research Letters, 33(19),
443 <https://doi.org/10.1029/2006GL027022>, 2006.

444 13.21. Kaplan, J.O., and Lau, K.H.K.^{1,2} World wide lightning location network (WWLLN) global lightning
445 climatology (WGLC) and time series, 2022 update, *Earth System Science Data*, 14(12), pp.5665-5670,
446 <https://doi.org/10.5281/zenodo.6007052>, 2022.

447 14.22. Kastman, J.S., Market, P.S., Fox, N.I., Foscato, A.L., and Lupo, A.R.: Lightning and rainfall
448 characteristics in elevated vs. surface based convection in the midwest that produce heavy rainfall, *Atmosphere*,
449 8(2), p.36, <https://doi.org/10.3390/atmos8020036>, 2017.

450 15.23. Katz, E. and Kalman, G.: The impact of environmental and geographical conditions on lightning
451 parameters derived from lightning location system in Israel, In Proceeding of the 10th International Symposium
452 on Lightning Protection, Curitiba, Brazil, November (pp. 9-13), 2009.

453 16.24. MacGorman, D.R., and Rust, W.D.: *The electrical nature of storms*, Oxford University Press, USA,
454 1998.

455 17.25. Maddox, R.A., Howard, K.W., Bartels, D.L., and Rodgers, D.M.: Mesoscale convective complexes in
456 the middle latitudes, In *Mesoscale meteorology and forecasting* (pp. 390-413), Boston, MA: American
457 Meteorological Society, 1986.

458 18.26. Mattos, E.V., and Machado, L.A.: Cloud-to-ground lightning and Mesoscale Convective Systems,
459 Atmospheric Research, 99(3-4), pp.377-390, <https://doi.org/10.1016/j.atmosres.2010.11.007>, 2011.

460 19.27. Mazur, V.^{1,2} Associated lightning discharges, *Geophysical Research Letters*, 9(11), pp.1227-1230,
461 <https://doi.org/10.1029/GL009i011p01227>, 1982.

462 20.28. Molion, L.C.B.: Amazonia rainfall and its variability, *Hydrology and water management in the humid
463 tropics*, Hufschmidt, M.M., Gladwell, J.S., Eds., pp.99-111, 1993.

464 21.29. Nobre, C.A., Obregón, G.O., Marengo, J.A., Fu, R., and Poveda, G.: Characteristics of Amazonian
465 climate: main features, *Amazonia and global change*, 186, pp.149-162, 2009.

466 22.30. Oda, P.S., Enoré, D.P., Mattos, E.V., Gonçalves, W.A., and Albrecht, R.I.: An initial assessment of the
467 distribution of total Flash Rate Density (FRD) in Brazil from GOES-16 Geostationary Lightning Mapper (GLM)
468 observations, *Atmospheric Research*, 270, p.106081, <https://doi.org/10.1016/j.atmosres.2022.106081>,
469 2022.

470 23.31. Ondrášková, A., Bór, J., Kostecký, P., and Rosenberg, L.: Peculiar transient events in the Schumann
471 resonance band and their possible explanation, *Journal of atmospheric and solar-terrestrial physics*, 70(6),
472 pp.937-946, <https://doi.org/10.1016/j.jastp.2007.04.013>, 2008.

473 24.32. Poelman, D.R., Schulz, W., Pedebay, S., Hill, D., Saba, M., Hunt, H., Schwalt, L., Vergeiner, C., Mata,
474 C., Schumann, C., and Warner, T.: Global ground strike point characteristics in negative downward lightning
475 flashes—Part 1: Observations, *Natural Hazards and Earth System Sciences Discussions*, 2021, pp.1-17,
476 <https://doi.org/10.5194/nhess-21-1909-2021>, 2021.

477 25.33. Rakov, V.A., A review of positive and bipolar lightning discharges, Bulletin of the American
478 Meteorological Society, 84(6), pp.767-776, <https://doi.org/10.1175/BAMS-84-6-767>, 2003.

479 34. Riemann-Campe, K., Fraedrich, K. and Lunkeit, F.: Global climatology of convective available potential energy
480 (CAPE) and convective inhibition (CIN) in ERA-40 reanalysis. Atmospheric Research, 93(1-3), pp.534-545,
481 <https://doi.org/10.1016/j.atmosres.2008.09.037>, 2009.

482 35. San Segundo, H., López, J.A., Pineda, N., Altube, P. and Montanya, J.: Sensitivity analysis of lightning stroke-
483 to-flash grouping criteria. Atmospheric Research, 242, pp.105023,
484 <https://doi.org/10.1016/j.atmosres.2020.105023>, 2020.

485 26.36. Scaff, L., Prein, A.F., Li, Y., Clark, A.J., Krogh, S.A., Taylor, N., Liu, C., Rasmussen, R.M., Ikeda, K.,
486 and Li, Z., Dryline characteristics in North America's historical and future climates, Climate Dynamics, 57(7),
487 pp.2171-2188, <https://doi.org/10.1007/s00382-021-05862-1>, 2021.

488 37. Setvák, M., Lindsey, D.T., Novák, P., Wang, P.K., Radová, M., Kerkmann, J., Grasso, L., Su, S.H., Rabin, R.M.,
489 Štáská, J. and Charvát, Z.: Satellite-observed cold-ring-shaped features atop deep convective clouds.
490 Atmospheric Research, 97(1-2), pp.80-96, <https://doi.org/10.1016/j.atmosres.2010.03.009>, 2010.

491 27.38. Shalev, S., Saaroni, H., Izsak, T., Yair, Y., and Ziv, B.: The spatio-temporal distribution of lightning
492 over Israel and the neighboring area and its relation to regional synoptic systems, Natural Hazards and Earth
493 System Sciences, 11(8), pp.2125-2135, <https://doi.org/10.5194/nhess-11-2125-2011>, 2011.

494 39. Shay-El, Y. and Alpert, P.: A diagnostic study of winter diabatic heating in the Mediterranean in relation to
495 cyclones. Quarterly Journal of the Royal Meteorological Society, 117(500), pp.715-747,
496 <https://doi.org/10.1002/qj.49711750004>, 1991.

497 28.40. Siingh, D., Gopalakrishnan, V., Singh, R.P., Kamra, A.K., Singh, S., Pant, V., Singh, R., and Singh,
498 A.K. :The atmospheric global electric circuit: an overview, Atmospheric Research, 84(2), pp.91-110,
499 <https://doi.org/10.1016/j.atmosres.2006.05.005>, 2007.

500 29.41. Strauss, C., Rosa, M.B. and Stephany, S.: Spatio-temporal clustering and density estimation of lightning
501 data for the tracking of convective events, Atmospheric Research, 134, pp.87-9,
502 <https://doi.org/10.1016/j.atmosres.2013.07.008>, 2013.

503 30.42. Tuttle, J.D. and Davis, C.A.: Corridors of warm season precipitation in the central United States,
504 Monthly Weather Review, 134(9), pp.2297-2317, <https://doi.org/10.1175/MWR3188.1>, 2006.

505 31.43. Vonnegut, B., Vaughan Jr, O.H., Brook, M., and Krehbiel, P.: Mesoscale observations of lightning from
506 space shuttle, Bulletin of the American Meteorological Society, 66(1), pp.20-29,
507 [https://doi.org/10.1175/1520-0477\(1985\)066%3C0020:MOOLFS%3E2.0.CO;2](https://doi.org/10.1175/1520-0477(1985)066%3C0020:MOOLFS%3E2.0.CO;2), 1985.

508 44. Wiens, K. C., and Suszcynsky, D. M.: Observed relationships among Narrow Bipolar Events, total lightning and
509 convective strength in Summer 2005 Great Plains thunderstorms. Second Conference on Meteorological
510 Applications of Lightning Data, AMS Annual Meeting, Poster P1.8, 2006.

511 32.45. Williams, E., Rosenfeld, D., Madden, N., Gerlach, J., Gears, N., Atkinson, L., Dunnemann, N.,
512 Frostrom, G., Antonio, M., Bazon, B., and Camargo, R.: Contrasting convective regimes over the Amazon:
513 Implications for cloud electrification, *Journal of Geophysical Research: Atmospheres*, 107(D20), pp.LBA-50,
514 <https://doi.org/10.1029/2001JD000380>, 2002.

515 33.46. Wright, J.S., Fu, R., Worden, J.R., Chakraborty, S., Clinton, N.E., Risi, C., Sun, Y., and Yin, L.:
516 Rainforest-initiated wet season onset over the southern Amazon, *Proceedings of the National Academy of
517 Sciences*, 114(32), pp.8481-8486, <https://doi.org/10.1073/pnas.1621516114>, 2017.

518 34.47. Wu, T., Wang, D., and Takagi, N.: Multiple-stroke positive cloud-to-ground lightning observed by the
519 FALMA in winter thunderstorms in Japan, *Journal of Geophysical Research: Atmospheres*, 125(20),
520 p.e2020JD033039, <https://doi.org/10.1029/2020JD033039>, 2020.

521 35.48. Yair, Y., Aviv, R., Ravid, G., Yaniv, R., Ziv, B., and Price, C.: Evidence for synchronicity of lightning
522 activity in networks of spatially remote thunderstorms, *Journal of atmospheric and solar-terrestrial physics*,
523 68(12), pp.1401-1415, <https://doi.org/10.1016/j.jastp.2006.05.012>, 2006.

524 36.49. Yair, Y.Y., Aviv, R., and Ravid, G.: Clustering and synchronization of lightning flashes in adjacent
525 thunderstorm cells from lightning location networks data, *Journal of Geophysical Research: Atmospheres*,
526 114(D9), <https://doi.org/10.1029/2008JD010738>, [2009a2009](#).

527 50. Yair, Y., Price, C., Ganot, M., Greenberg, E., Yaniv, R., Ziv, B., Sherez, Y., Devir, A., Bór, J.Z. and Sátori, G.:
528 Optical observations of transient luminous events associated with winter thunderstorms near the coast of Israel.
529 Atmospheric Research, 91(2-4), pp.529-537, <https://doi.org/10.1016/j.atmosres.2008.06.018>, 2009b.

530 37.51. Yair, Y.: Lightning hazards to human societies in a changing climate, *Environmental research letters*,
531 13(12), p.123002, DOI 10.1088/1748-9326/aaea86, 2018.

532 38.52. Zhu, Y., Stock, M., Lapierre, J., and DiGangi, E.: Upgrades of the Earth networks total lightning
533 network in 2021, *Remote sensing*, 14(9), p.2209, <https://doi.org/10.3390/rs14092209>, 2022.

534 39.53. Ziegler, C.L., and Rasmussen, E.N.: The initiation of moist convection at the dryline: forecasting issues
535 from a case study perspective, *Weather and forecasting*, 13(4), pp.1106-1131, [https://doi.org/10.1175/1520-0434\(1998\)013%3C1106:TIOMCA%3E2.0.CO;2](https://doi.org/10.1175/1520-
536 0434(1998)013%3C1106:TIOMCA%3E2.0.CO;2), 1998.

537 40.54. Ziv, B., Dayan, U., and Sharon, D.: A mid-winter, tropical extreme flood-producing storm in southern
538 Israel: synoptic scale analysis, *Meteorology and Atmospheric Physics*, 88, pp.53-63,
539 <https://doi.org/10.1007/s00703-003-0054-7>, 2005.

540 41.55. Zoghzoghy, F.G., Cohen, M.B., Said, R.K., and Inan, U.S.: Statistical patterns in the location of natural
541 lightning, *Journal of Geophysical Research: Atmospheres*, 118(2), pp.787-796,
542 <https://doi.org/10.1002/jgrd.50107>, 2013.